Phase Behavior of Telechelic Polyisobutylene in Subcritical and Supercritical Fluids. 4. SAFT Association Parameters from FTIR for Blank, Monohydroxy, and Dihydroxy PIB 200 in Ethane, Carbon Dioxide, and Chlorodifluoromethane

Christopher J. Gregg,[†] Fred P. Stein,*[,‡] and Maciej Radosz[§]

BOC Process Plants, Murray Hill, New Jersey 07974, Department of Chemical Engineering, Lehigh University, Bethlehem Pennsylvania 18015, and Department of Chemical Engineering, Louisiana State University

Received: July 24, 1998; In Final Form: October 22, 1998

Phase-boundary pressures were measured for binary subcritical and supercritical fluid solutions of nonfunctional (referred to as blank), monohydroxy, and dihydroxy polyisobutylenes (200 g/mol) in ethane, carbon dioxide, and chlorodifluoromethane from −50 to 200 °C up to 400 bar. As hydroxy groups were added to (blank) polyisobutylene, the phase-boundary pressure was found to increase due to intermolecular self- or cross-association. With carbon dioxide rather than ethane as the solvent, these boundaries are (1) 2−3 times lower in pressure and (2) shift differently than those reported in the literature for 2,5-hexanediol [HO−PE−OH (100)]. To examine these differences, the association parameters for the statistical associating fluid theory model (SAFT) were determined from spectroscopic data and then used to calculate phase boundaries and aggregate size for HO−PIB−OH (200) and HO−PE−OH (100). The SAFT analysis suggests that the steric hindrance due to the methyl branches in PIB decreases the aggregate size and hence lowers the phase-boundary pressure.

Introduction

Molecules that cluster or aggregate through hydrogen bonds or polar−polar interactions can have fluid-phase properties that differ drastically from those of their nonassociating counterparts. For example, ethane solutions of methanol and carbon dioxide solutions of 2,5-hexanediol[1,2] exhibit large deviations from ideality. These two systems exhibit liquid−liquid immiscibility with phase-boundary pressures exceeding 1000 bar. In contrast, their nonassociating analogues, ethane solutions of methane[3] and carbon dioxide solutions of hexane,[4,5] exhibit vapor−liquid equilibria with phase-boundary pressures below 200 bar. Such order of magnitude differences in fluid-phase properties have attracted a great deal of experimental[6−12] and theoretical[13−17] interest in studying associating systems.

In this work, our objective was to measure the phase-boundary pressures of nonfunctional (referred to as blank), monohydroxy, and dihydroxy polyisobutylene (PIB) in ethane, carbon dioxide, and chlorodifluoromethane. These model PIB oligomers have molecular weights near 200 g/mol and are referred to as PIB (200). The data collected in this work were compared to the literature data for 2,5-hexanediol [HO−PE−OH (100)][1] and were analyzed using the statistical associating fluid theory (SAFT) model.

Phase Equilibrium Measurements

Solvents and Polymers. Three supercritical fluid solvents were selected to study the various degrees of self-association and cross-association between PIB (200) and solvent molecules, namely, ethane, carbon dioxide, and chlorodifluoromethane. Ethane is inert, carbon dioxide is quadrupolar (4.00 $erg^{1/2}$ $cm^{5/2}$ $\times 10^{26}$), and chlorodifluoromethane is polar (1.48 D)[18] and can cross-associate.

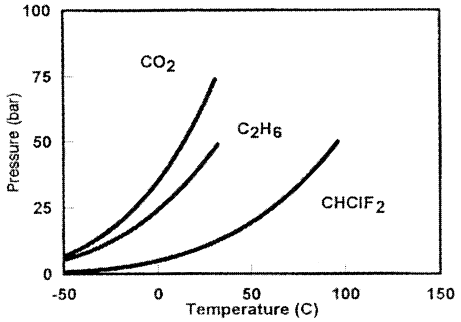

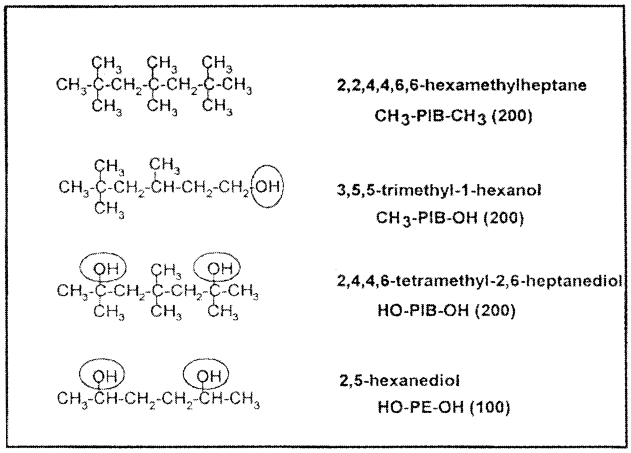

Figure 1. (Top) vapor pressure curves for ethane (C_2H_6), carbon dioxide (CO_2), and chlorodifluoromethane ($CHClF_2$). (Bottom) illustrative chemical structures for 2,2,4,4,6,6-hexamethylheptane [CH_3−PIB−CH_3 (200)], 3,5,5-trimethyl-1-hexanol [CH_3−PIB−OH (200)], 2,4,4,6-tetra-methyl-2,6-heptanediol [HO−PIB−OH (200)], and 2,5-hexanediol [HO−PIB−OH (100)].

* To whom correspondence should be addressed.
[†] BOC Process Plants.
[‡] Lehigh University.
[§] Louisiana State University.

10.1021/jp983157a CCC: $18.00
Published on Web 01/29/1999

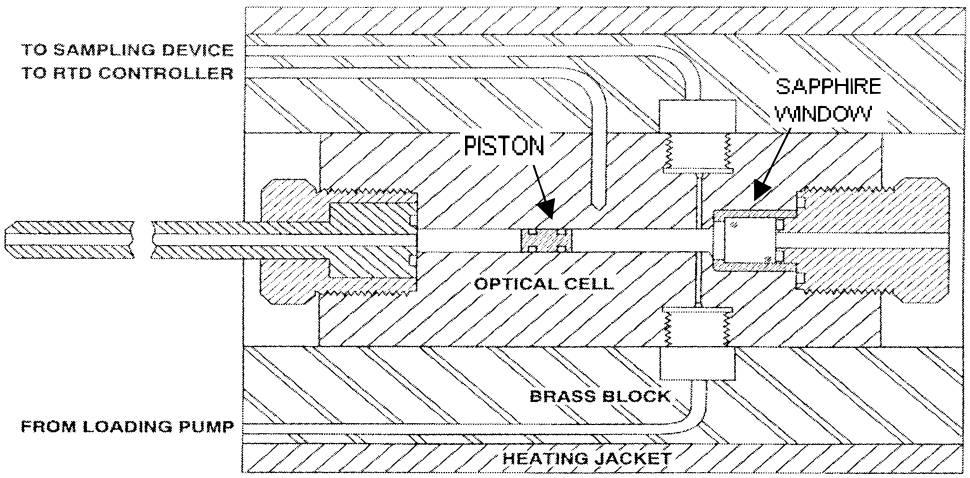

Figure 2. Schematic of the high-pressure optical cell used to measure cloud points. Key parts include the cell body, moveable piston, brass block, and heating jacket.

As illustrated in Figure 1 (upper), carbon dioxide and ethane have similar critical temperatures while ethane and chlorodifluoromethane have similar critical pressures. These fluids were purchased from Matheson, with a known minimum purity of 99.8%, and were used without further purification.

Three model PIB oligomers were selected for this study, blank, monohydroxy, and dihydroxy polyisobutylenes [PIB (200)]. As schematically illustrated in Figure 1 (lower), the PIB (200) oligomers have nearly the same backbone with either zero, one, or two terminal hydroxy groups. This figure also illustrates the structure for a model polyethylene oligomer diol, 2,5-hexanediol HO−PE−OH (100).

The CH_3−PIB−CH_3 (200), synthetically prepared by carbocationic polymerization,[19,20] is a mixture of 68% main product and 32% isomers; the isomers have similar structure and the same molecular weight as the main components and, hence, should not differ much in phase behavior. The CH_3−PIB−OH (200) was purchased from Aldrich and found to be 93.6% pure, and the HO−PIB−OH (200) was synthetically prepared[20] with a purity greater than 99%+; the melting point range was found to be 90.8−91.6 °C.

Apparatus and Procedure. The phase-boundary pressures were measured using a variable-volume batch cell that has been discussed elsewhere in detail.[21] As shown in Figure 2, the cell is equipped with a sapphire window; moveable piston; feed, sampling, and RTD ports; brass block; and heating jacket. The key components are the window and piston that allow visual observation of the phase transition and continuous control of cell volume and pressure at constant composition. An external heating jacket that fits over a cylindrical brass sleeve is used to heat the cell; the inner cell-bore temperature can be controlled to within ±0.1 °C.

In operation, a known amount of the solute and solvent are loaded into the cell. The stirred contents are then pressurized into a one-phase homogeneous solution by moving the piston toward the window. After the temperature is adjusted and equilibrium established, the solution pressure is slowly lowered by moving the piston away from the window to promote phase separation. At the onset of phase separation, the cell pressure is recorded as either bubble- or dew-point, depending upon the formation of a light phase (bubble-point) or a heavy phase (dew-point).[22] This process is repeated at various temperatures to produce a pressure−temperature isopleth curve.

Phase-Boundary Pressures for Associating PIB (200) in Ethane, Carbon Dioxide, and Chlorodifluoromethane. In all,

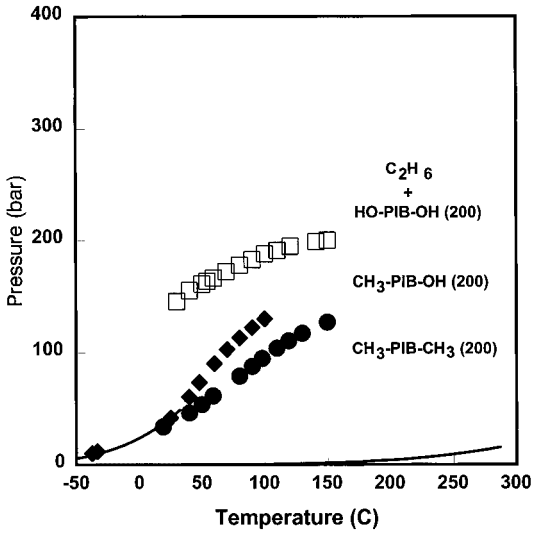

Figure 3. Binary pressure−temperature diagram for ethane (C_2H_6) solutions of 11.0 mol % CH_3−PIB−CH_3 (200), 11.0 mol % CH_3−PIB−OH (200), and 6.7 mol % HO−PIB−OH (200): solid curves are the vapor pressure of ethane and CH_3−PIB−OH (200); circles are the data for CH_3−PIB−CH_3 (200); diamonds are the data for CH_3−PIB−OH (200); squares are the data for HO−PIB−OH (200).

13 isopleth curves were measured for CH_3−PIB−CH_3 (200), CH_3−PIB−OH (200), and HO−PIB−OH (200) in ethane, shown in Figure 3, in carbon dioxide, shown in Figure 4, and in chlorodifluoromethane, shown in Figure 5. The experimental data are listed in Tables 1−3. In each of the figures to follow, the pressure−temperature curves (symbols) indicate the miscibility limit; the area above the curve (symbols) is the one-phase region, and that below the curve (symbols) is the two-phase region. The vapor pressure curve for the solvent and the estimated vapor pressure curve for CH_3−PIB−OH (200) are also shown for reference. In all the figures in this work, open symbols refer to dew-point-like phase transitions whereas filled symbols refer to bubble-point-like phase transitions.

Figure 3 shows the phase diagram for 11.0 mol % CH_3−PIB−CH_3 (200) in ethane. The behavior is of type A, similar to other ethane−hydrocarbons systems.[23−26] Type A refers to systems with a low degree of asymmetry that are characterized by a continuous vapor−liquid (VL) critical locus connecting the critical point of the solute to the critical point of the solvent.[27]

With the addition of one hydroxy group, CH_3−PIB−CH_3 (200) becomes CH_3−PIB−OH (200), the phase boundary shifts

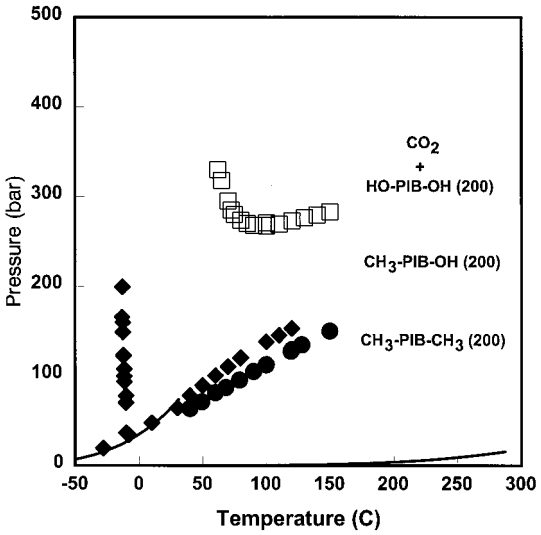

Figure 4. Binary pressure−temperature diagram for carbon dioxide (CO_2) solutions of 20.4 mol % $CH_3-PIB-CH_3$ (200), 21.6 mol % $CH_3-PIB-OH$ (200), and 7.6 mol % HO−PIB−OH (200): solid curves are the vapor pressures of carbon dioxide and $CH_3-PIB-OH$ (200); circles are the data for $CH_3-PIB-CH_3$ (200); diamonds are the data for $CH_3-PIB-OH$ (200); squares are the data for HO−PIB−OH (200).

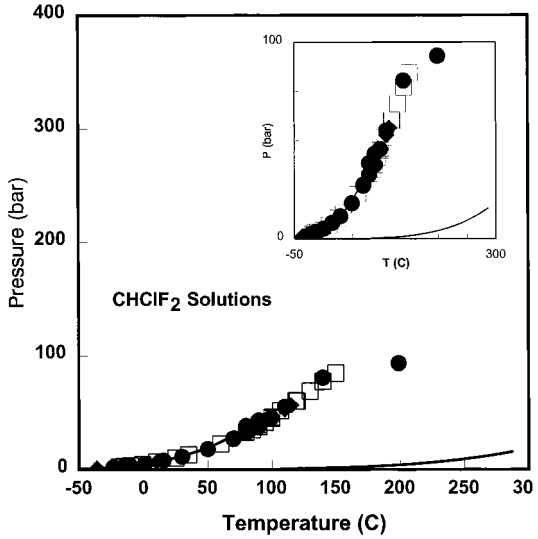

Figure 5. Binary pressure−temperature diagram for chlorodifluoromethane ($CHClF_2$) solutions of 5.4 mol % $CH_3-PIB-CH_3$ (200), 6.4 and 21.6 mol % $CH_3-PIB-OH$ (200), and 7.6 mol % HO−PIB−OH (200): solid curves are the vapor pressures of chlorodifluoromethane and $CH_3-PIB-OH$ (200); circles are the data for $CH_3-PIB-CH_3$ (200); diamonds are the data for $CH_3-PIB-OH$ (200); squares are the data for HO−PIB−OH (200); inset shows expanded pressure scale.

to slightly higher pressures, as shown by the curve for 11.0 mol % polymer. The addition of a second hydroxy group approximately doubles the phase-boundary pressures, relative to $CH_3-PIB-CH_3$ (200) and leads to type-B behavior (discontinuous critical locus). The data for 6.7 mol % HO−PIB−OH (200) are of the dew-point type (open symbols), whereas the data for both 11.0 mol % $CH_3-PIB-CH_3$ (200) and 11.0 mol % $CH_3-PIB-OH$ (200) are of the bubble-point (solid symbols) type.

Figure 4 illustrates the phase boundary data for 20.4 mol % $CH_3-PIB-CH_3$ (200), 21.6 mol % $CH_3-PIB-OH$ (200), and 7.6 mol % HO−PIB−OH (200) in carbon dioxide. Carbon dioxide solutions of $CH_3-PIB-CH_3$ (200) exhibit type-A behavior with no liquid−liquid (LL) immiscibility above −45 °C, which is consistent with the literature.[28−31] In contrast, carbon dioxide solutions of $CH_3-PIB-OH$ (200) exhibit liquid−liquid (L−L) immiscibility (Type B) and have an upper critical end point (UCEP) that is projected onto the carbon dioxide vapor pressure curve near −10.1 °C; this value is closer to the −13.5 °C value for 2-hexanol[1] than to the 39.5 °C value for 1-hexanol.[32]

The addition of the second hydroxy group shifts the phase boundary to even higher pressures and from liquid−liquid type-B to upper−lower critical solution temperature (U-LCST). As shown in Figure 4, the phase-boundary pressures for HO−PIB−OH (200) are nearly double those of the corresponding

TABLE 1: Experimental Phase-Boundary Pressures for R−PIB−R (200) in Ethane

feed R−PIB−R (mol %)		T (±0.1 °C)	P (±1.0 bar)	type[a]
CH3−PIB−CH3	10.95	150.0	126.9	VL(BP)
	10.95	130.0	117.1	VL(BP)
	10.95	119.2	110.4	VL(BP)
	10.95	109.8	103.7	VL(BP)
	10.95	98.1	94.7	VL(BP)
	10.95	90.0	87.6	VL(BP)
	10.95	80.0	79.0	VL(BP)
	10.95	58.8	61.4	VL(BP)
	10.95	50.0	53.6	VL(BP)
	10.95	40.0	46.1	VL(BP)
	10.95	19.1	33.8	VL(BP)
CH3−PIB−OH	11.01	100.0	130.0	VL(BP)
	11.01	90.0	122.3	VL(BP)
	11.01	80.0	113.2	VL(BP)
	11.01	70.0	102.8	VL(BP)
	11.01	59.7	90.1	VL(BP)
	11.01	47.8	73.2	VL(BP)
	11.01	39.8	60.3	VL(BP)
	11.01	33.7	50.5	VL(BP)
	11.01	25.0	41.7	VL(BP)
	11.01	−33.5	11.7	VL(BP)
	11.01	−42.9	9.2	VL(BP)
HO−PIB−OH	10.94	150.0	199.3	VL(BP)
	10.94	138.3	197.6	VL(BP)
	10.94	130.0	195.9	VL(BP)
	10.94	95.0	183.6	VL(BP)
	10.94	90.0	181.3	VL(BP)
	10.94	79.3	176.2	VL(BP)
	10.94	70.0	171.6	VL(BP)
	10.94	50.0	159.9	VL(BP)
HO−PIB−OH	6.66	100.1	193.4	VL(DP)
	6.66	87.0	189.1	VL(DP)
	6.66	77.8	185.0	VL(DP)
	6.66	75.0	185.0	VL(DP)
	6.66	70.0	183.4	VL(DP)
	6.66	60.0	180.2	VL(DP)
	6.66	47.3	176.0	VL(DP)
	6.66	45.0	175.1	VL(DP)
	6.66	40.0	173.4	VL(DP)
	6.66	29.5	169.3	VL(DP)
	6.66	23.3	166.6	VL(DP)
HO−PIB−OH	5.82	140.0	198.7	VL(DP)
	5.82	120.4	194.6	VL(DP)
	5.82	110.0	191.1	VL(DP)
	5.82	100.0	187.9	VL(DP)
	5.82	90.0	182.7	VL(DP)
	5.82	80.0	177.9	VL(DP)
	5.82	69.2	172.1	VL(DP)
	5.82	59.2	166.4	VL(DP)
	5.82	54.1	163.5	VL(DP)
	5.82	50.0	161.0	VL(DP)
	5.82	40.0	155.3	VL(DP)
	5.82	30.0	143.0	VL(DP)

[a] Phase transition type: VL ≡ vapor−liquid; LL ≡ liquid−liquid; BP ≡ bubble-point-like transition; DP ≡ dew-point-like transition.

TABLE 2: Experimental Phase-Boundary Pressures for R−PIB−R (200) in Carbon Dioxide

feed R−PIB−R (mol %)		T (±0.1 °C)	P (±1.0 bar)	type[a]
CH3−PIB−CH3	20.38	150.0	149.8	VL(BP)
	20.38	128.0	134.5	VL(BP)
	20.38	120.3	129.2	VL(BP)
	20.38	119.4	127.3	VL(BP)
	20.38	100.0	112.8	VL(BP)
	20.38	90.0	104.8	VL(BP)
	20.38	79.0	95.4	VL(BP)
	20.38	68.3	87.0	VL(BP)
	20.38	60.0	81.2	VL(BP)
	20.38	49.3	71.1	VL(BP)
	20.38	40.0	63.7	VL(BP)
CH3−PIB−OH	21.56	120.0	152.6	VL(BP)
	21.56	110.0	145.1	VL(BP)
	21.56	100.0	137.7	VL(BP)
	21.56	80.0	120.0	VL(BP)
	21.56	79.7	119.5	VL(BP)
	21.56	70.0	110.2	VL(BP)
	21.56	60.0	100.1	VL(BP)
	21.56	49.9	89.2	VL(BP)
	21.56	40.0	77.9	VL(BP)
	21.56	30.1	64.4	VL(BP)
	21.56	10.0	47.7	VL(BP)
	21.56	−8.0	34.2	VL(BP)
	21.56	−10.0	36.6	VL(BP)
	21.56	−10.1	70.2	LL(BP)
	21.56	−10.2	77.6	LL(BP)
	21.56	−11.4	93.4	LL(BP)
	21.56	−11.5	99.4	LL(BP)
	21.56	−11.6	107.6	LL(BP)
	21.56	−12.0	122.1	LL(BP)
	21.56	−12.2	122.9	LL(BP)
	21.56	−12.5	148.5	LL(BP)
	21.56	−12.6	159.5	LL(BP)
	21.56	−13.0	199.3	LL(BP)
	21.56	−13.2	265.2	LL(BP)
HO−PIB−OH	7.60	150.0	283.0	LL(NC)
	7.60	140.0	279.6	LL(NC)
	7.60	130.0	276.5	LL(NC)
	7.60	120.0	273.2	LL(NC)
	7.60	110.0	269.4	LL(NC)
	7.60	100.0	267.5	LL(NC)
	7.60	100.0	270.7	LL(NC)
	7.60	90.0	268.2	LL(NC)
	7.60	85.0	269.9	LL(BP)
	7.60	80.0	273.5	LL(BP)
	7.60	75.0	279.9	LL(BP)
	7.60	72.5	285.1	LL(BP)
	7.60	70.0	295.1	LL(BP)
	7.60	64.8	317.8	LL(BP)
	7.60	62.0	329.5	LL(BP)

[a] Phase transition type: VL ≡ vapor−liquid; LL ≡ liquid−liquid; BP ≡ bubble-point-like transition; DP ≡ dew-point-like transition; NC ≡ near critical.

nonassociating CH_3−PIB−CH_3 (200) system. The UCST branch of the phase boundary is below 50 °C.

In chlorodifluoromethane solutions, shown in Figure 5, the phase-boundary pressures for CH_3−PIB−CH_3 (200), CH_3−PIB−OH (200), and HO−PIB−OH (200) essentially coincide over the entire temperature range investigated because chlorodifluoromethane is a good solvent for polar solutes.[33] All three solutions exhibit vapor−liquid type-A behavior and no signs of liquid−liquid immiscibility for CH_3−PIB−CH_3 (200) and CH_3−PIB−OH (200) above −36 °C. However, a solid−liquid−vapor (SLV) transition (see Table 3) was observed for HO−PIB−OH (200) at −19 °C.

The phase-boundary shifts for CH_3−PIB−OH (200) and HO−PIB−OH (200), relative to CH_3−PIB−CH_3 (200), can be explained by intermolecular association. For example, in ethane and carbon dioxide, the shift to higher pressures, as hydroxy groups are added to PIB (200), is due to the formation of

TABLE 3: Experimental Phase-Boundary Pressures for R−PIB−R (200) in Chlorodifluoromethane

feed R−PIB−R (mol %)		T (±0.1 °C)	P (±1.0 bar)	type[a]
CH3−PIB−CH3	5.40	199.1	93.1	VL(DP)
	5.40	139.9	80.6	VL(BP)
	5.40	110.2	55.1	VL(BP)
	6.41	100.2	45.6	VL(BP)
	5.40	99.7	45.6	VL(BP)
	5.40	99.3	43.3	VL(BP)
	6.41	90.0	37.6	VL(BP)
	5.40	89.8	38.5	VL(BP)
	6.41	80.0	32.5	VL(BP)
	5.40	79.9	32.5	VL(BP)
	5.40	70.3	27.5	VL(BP)
	5.40	70.0	27.4	VL(BP)
	6.41	70.0	27.0	VL(BP)
	6.41	50.0	18.1	VL(BP)
	6.41	30.0	11.4	VL(BP)
	6.41	15.6	8.0	VL(BP)
	6.41	1.0	5.2	VL(BP)
	6.41	−10.6	3.5	VL(BP)
	6.41	−15.1	3.1	VL(BP)
	6.41	−23.3	2.1	VL(BP)
CH3−PIB−OH	15.39	149.7	73.5	VL(BP)
	15.39	140.0	67.2	VL(BP)
	15.39	130.5	59.9	VL(BP)
	15.39	120.0	53.2	VL(BP)
	15.39	109.8	46.7	VL(BP)
	15.39	100.0	40.5	VL(BP)
	15.39	90.0	34.6	VL(BP)
	15.39	80.0	29.3	VL(BP)
	15.39	75.0	26.8	VL(BP)
	15.39	60.0	20.1	VL(BP)
	15.39	47.8	15.8	VL(BP)
	15.39	40.0	13.2	VL(BP)
	15.39	30.0	10.6	VL(BP)
	8.98	115.0	56.4	VL(BP)
	8.98	110.0	52.7	VL(BP)
	8.98	100.0	45.5	VL(BP)
	8.98	90.0	38.8	VL(BP)
	8.98	80.0	32.4	VL(BP)
	8.98	70.0	27.3	VL(BP)
	8.98	50.0	17.7	VL(BP)
	8.98	30.0	11.4	VL(BP)
	8.98	10.0	6.7	VL(BP)
	8.98	−23.5	2.1	VL(BP)
	8.98	−36.2	1.3	VL(BP)
HO−PIB−OH	8.01	150.0	84.5	VL(BP)
	8.01	140.0	77.3	VL(BP)
	8.01	130.0	68.8	VL(BP)
	8.01	120.0	60.0	VL(BP)
	8.01	118.9	60.4	VL(BP)
	8.01	107.0	51.6	VL(BP)
	8.01	100.0	45.1	VL(BP)
	8.01	95.0	41.6	VL(BP)
	8.01	90.0	37.6	VL(BP)
	8.01	85.0	35.2	VL(BP)
	8.01	80.0	33.0	VL(BP)
HO−PIB−OH	6.49	100.0	46.2	VL(BP)
	6.49	90.0	39.5	VL(BP)
	6.49	80.0	32.9	VL(BP)
	6.49	60.0	22.5	VL(BP)
	6.49	35.0	13.2	VL(BP)
	6.49	25.0	10.4	VL(BP)
	6.49	10.0	6.8	VL(BP)
	6.49	−0.9	4.5	VL(BP)
	6.49	−10.6	3.4	VL(BP)
	6.49	−15.1	3.0	VL(BP)
	6.49	−19.0	2.5	SLV(BP)

[a] Phase transition type: VL ≡ vapor−liquid; LL ≡ liquid−liquid; BP ≡ bubble-point-like transition; DP ≡ dew-point-like transition; NC ≡ near critical.

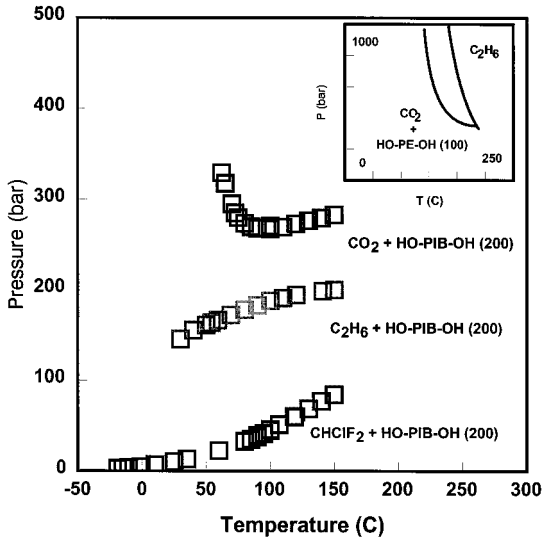

Figure 6. Binary pressure−temperature diagram for HO−PIB−OH (200) in carbon dioxide (CO_2), ethane (C_2H_6), and chlorodifluoromethane ($CHClF_2$) showing type-B (upper curve) through type-A (lower curve) behavior. Inset shows literature data of HO−PE−OH (100) (2,5-hexanediol) in carbon dioxide and ethane.[1]

hydrogen-bonded polymer aggregates. These aggregates form by self-association and increase the system asymmetry, which is known to shift phase boundaries to higher pressures.[1,22,34] The lack of such a shift for the chlorodifluoromethane solution is due to the cross-association (between the solvent and the polymer) that inhibits the PIB hydroxy groups from self-associating.

Comparing HO−PIB−OH (200) and HO−PE-OH (100). Figure 6 shows the phase boundaries for HO−PIB−OH (200) in ethane, carbon dioxide, and chlorodifluoromethane and (inset) for HO−PE−OH (100) in ethane and carbon dioxide. Figure 6 illustrates two key differences between these diols. (1) The phase-boundary pressures for HO−PE−OH (100) in either ethane or carbon dioxide are much higher than those for HO−PIB−OH (200). (2) The phase boundary pressures for carbon dioxide solutions of HO−PE−OH (100) are lower than those for ethane, which is opposite to the behavior exhibited by HO−PIB−OH (200). This difference in behavior suggests that, relative to ethane, carbon dioxide is a better solvent (requires lower pressures) for HO−PE−OH (100) but is a poorer solvent (requires higher pressures) for HO−PIB−OH (200), which is counterintuitive.

To elucidate these differences between the two diol systems, the statistical associating fluid theory model (SAFT) was used to calculate the phase boundaries for HO−PIB−OH (200) and HO−PE−OH (100) in ethane and carbon dioxide solutions. The approach is to (1) determine independently the self-association and cross-association parameters from spectroscopic data, (2) estimate the binary interaction parameter (k_{ij}) for these solutions, and (3) calculate the average aggregate size of HO−PIB−OH (200) and HO−PE−OH (100) in ethane and carbon dioxide near the phase boundary.

Saft Association Parameters from Spectroscopic Data

SAFT Model. The SAFT equation of state is expressed in terms of the residual Helmholtz energy that consists of contributions from repulsive forces (hard sphere), mean-field forces (dispersive), chain formation (covalent bonds), and association (short-lived clusters). These contributions are characterized by three nonassociation and two association parameters. The three

TABLE 4: SAFT Pure Component and Association Parameters

compound	molar mass (g/mol)	m (segments)	v^{00} (cm^3/seg)	u^0/k (K)
CO_2	44.0	1.417	13.59	216.08
C_2H_6	30.1	1.945	14.46	191.45
t-butyl alcohol	58.2	3.458	12.60	191.11
HO−PE−OH (100)[a]	118.1	4.724	12.48	202.72
dodecanol	186.3	8.921	11.86	205.93
HO−PIB−OH (200)	188.3	5.581	12.00	225.00

	self-association OH···OH		cross-association O═C═O···HO	
system	ϵ/k (K)	κ	ϵ/k (K)	κ
t-butanol	2752	0.0058	1750	0.0180
HO−PE−OH (100)[a]	2752	0.0200	1750	0.0180
dodecanol	2752	0.0200	1750	0.0180
HO−PIB−OH (200)	2752	0.0058	1750	0.0180

[a] HO−PE−OH (100) is symbolic for 2,5-hexanediol.

nonassociation parameters are m, the number of segments per molecule, v^{00}, the temperature-independent segment volume in cm^3/mol of segments, and u/k, the segment energy in Kelvin (k = Boltzmann constant). The two association parameters are κ, dimensionless bond volume, and ϵ/k, association energy in Kelvin (k = Boltzmann constant).

The details of the equation, its extension to fluid mixtures via the vdW1 mixing rules, and the terminology used in this work are available in the literature.[35,36] Application examples include nonassociating systems, such as polynuclear aromatics,[37] long-chain *n*-alkanes,[38] and polymers.[34,39] In this work, the nonassociation parameters for HO−PIB−OH (200) and HO−PE-OH (100) were estimated from the Huang−Radosz correlation[35] but the association parameters were derived from spectroscopic data of model binary systems. Table 4 lists these parameters.

Self-Association Parameters from Ethane−Dodecanol Spectroscopic Data. The non-hydrogen-bonded (referred to as monomer) mole fraction of dodecanol in subcritical and supercritical ethane have been measured using infrared (IR) techniques.[40−44] These data are related to the SAFT association parameters through an expression for the fraction of monomers, e.g. molecules i not bonded at site A, (X^{A_i}), which is given by[15]

$$X^{A_i} = [1 + N_{Av}\sum_{j=1}^{NC\,sites}\sum_{B_j}\rho_j X^{B_j}\Delta^{A_iB_j}]^{-1} \quad (1)$$

where $\Delta^{A_iB_j}$ is the bond strength that depends on the SAFT association parameters and describes the interaction of site A on species i with site B on species j; ρ_j is the number density of species j; $\sum_{B_j}^{sites}$ sums over all the associating sites A_j, C_j, D_j, (on species j) ...; $\sum_{j=1}^{nc}$ sums over all the components. N_{Av} is Avogadro's number.

When eq 1 is applied to a two-site (A for hydrogen and B for oxygen) dodecanol molecule (component 1) in solution with a zero-site ethane molecule (component 2), assuming that dodecanol self-associates through AB and not through AA or BB interactions ($\Delta^{A_1B_1} \neq 0$, $\Delta^{A_1A_1} = \Delta^{B_1B_1} = 0$), eq 1 becomes

$$X^{A_1} = [1 + N_{Av}[\rho_1 X^{B_1}\Delta^{A_1B_1}]]^{-1} \quad (2)$$

Equation 2 is further simplified by realizing that $\rho_1 N_{Av} = X_1\rho_n$

and $X^{A_1} = X^{B_1}$, as follows:

$$X^{A_1} = \frac{-1 + \sqrt{1 + 4\rho_n X_1 \Delta^{A_1B_1}}}{2X_1\rho_n\Delta^{A_1B_1}} \quad (3)$$

In eq 3, X_1 is the apparent mole fraction of dodecanol and ρ_n is the molar number density. $\Delta^{A_1B_1}$ is given as

$$\Delta^{A_1B_1} = g_{11}(\sigma_{11})\kappa^{A_1B_1}[e^{\frac{\epsilon^{A_1B_1}}{kT}} - 1]{\sigma_{11}}^3 \quad (4)$$

where $\kappa^{A_1B_1}$ and $\epsilon^{A_1B_1}$ are the self-association volume and energy, $g_{11}(\sigma_{11})$ is the solute−solute pair correlation function, evaluated at contact, and σ_{11} is the hard-sphere segment diameter. The probability of a dodecanol molecule having both sites A and B free[45] is equal to $X^{A_1}X^{B_1}$. This value, multiplied by the apparent mole fraction X_1, gives the monomer mole fraction of dodecanol, which was equated to the measured values.[42] The self-association $\kappa^{A_1B_1}$ and $\epsilon^{A_1B_1}$ parameters (Table 4) were adjusted to make the SAFT predicted monomer mole fraction agree with that derived from the spectroscopic data.[42]

Cross-Association Parameters from Carbon Dioxide−Dodecanol Spectroscopic Data. In carbon dioxide solutions of dodecanol, two types of association exist, the self-association of dodecanol and the cross-association[42] between carbon dioxide and dodecanol. Thus, an expression must be developed that relates the fraction of nonbonded SAFT sites to the (1) non-hydrogen-bonded dodecanol (free alcohol molecule) and (2) the cross-associated carbon dioxide−dodecanol aggregate (1:1 CO_2−alcohol complex). Fulton et al.[42] consider both as monomers (non-hydrogen-bonded).

The procedure is similar to that outlined for ethane solutions of dodecanol, but here, a third site (site C) is assigned to the quadrupole moment of carbon dioxide. The expanded form of eq 1 becomes

$$X^{A_1} = [1 + N_{av}\{\rho_1 X^{B_1}\Delta^{A_1B_1}\} + N_{av}\{\rho_2 X^{C_2}\Delta^{A_1C_2}\}]^{-1} \quad (5)$$

where $\Delta^{A_1B_1}$ represents the self-associating interactions of dodecanol and $\Delta^{A_1C_2}$ represents the cross-associating interactions between carbon dioxide and dodecanol ($\Delta^{C_2A_1}$, $\Delta^{A_1C_2}$, $\Delta^{C_2C_2}$, and $\Delta^{C_2B_1} = O$). X^{B_1} is the fraction of dodecanol molecules not bonded at site B,

$$X^{B_1} = [1 + N_{av}\{\rho_1 X^{A_1}\Delta^{A_1B_1}\}]^{-1} \quad (6)$$

and X^{C_2} is the fraction of carbon dioxide molecules not bonded at site C,

$$X^{C_2} = [1 + N_{av}\{\rho_1 X^{A_1}\Delta^{A_1C_2}\}]^{-1} \quad (7)$$

Substituting eqs 6 and 7 into eq 5 results in an expression that is cubic in X^{A_1} and has two unknowns $\Delta^{A_1B_1}$ and $\Delta^{A_1C_2}$.

$$(N_{av}\rho_1)^2\Delta^{A_1B_1}\Delta^{A_1C_2}(X^{A_1})^3 + [{N_{av}}^2\rho_1\rho_2\Delta^{A_1B_1}\Delta^{A_1C_2} + {N_{AV}}^2\rho_1(\Delta^{A_1C_2} + \Delta^{A_1B_1})](X^{A_1})^2 + [1 + N_{av}\Delta^{A_1C_1}(\rho_2 - \rho_1)](X^{A_1}) - 1 = 0 \quad (8)$$

Assuming that $\Delta^{A_1B_1}$ is independent of $\Delta^{A_1C_2}$ and that $\Delta^{A_1B_1}$ determined for the ethane and dodecanol system can be used to describe $\Delta^{A_1B_1}$ in the carbon dioxide−dodecanol system, eq 8 then reduces to one equation with one unknown, $\Delta^{A_1C_2}$. Similar to eq 4, $\Delta^{A_1C_2}$ is defined as

$$\Delta^{A_1C_2} = g_{12}(\sigma_{12})\kappa^{A_1C_2}[e^{\frac{\epsilon^{A_1C_2}}{kT}} - 1]{\sigma_{12}}^3 \quad (9)$$

where $\kappa^{A_1C_2}$ is the cross-association bond volume and $\epsilon^{A_1C_2}$ is the cross-association bond energy. $g_{12}\sigma_{12}$ is the hard-sphere pair correlation function evaluated at contact, $N_{Av}\rho_1$ and $N_{Av}\rho_2$ are the molar densities (in eq 8), and σ_{12} is the hard-sphere diameter where index 1 is designated for dodecanol and index 2 is designated for carbon dioxide.

The probability of both sites A (hydrogen) and B (oxygen) on dodecanol being free is $X^{A_1}X^{B_1}$ (on the basis of arguments found in Jackson et al. 1988), and the probability of a free site B (oxygen on dodecanol) on a bonded AC (hydrogen−quadrupole) complex is $X^{B_1}(1 - X^{C_2})$. The mole number (n) of these two species in carbon dioxide solutions

$$n_{monomer} = (X^{A_1}X^{B_1})n_{dodecanol} + X^{B_1}(1 - X^{C_2})n_{carbon\ dioxide} \quad (10)$$

Given $\Delta^{A_1C_2}$, that is, guessing the cross-association $\kappa^{A_1C_2}$ and $\epsilon^{A_1C_2}$ and knowing g_{12} (from SAFT), X^{A_1} can be determined numerically from eq 8; X^{A_1} can then be substituted into eqs 6 and 7 to give X^{B_1} and X^{C_1}. These values, in turn, were used in eq 10 to give the SAFT monomer mole fraction. The cross-association parameters (Table 4) $\kappa^{A_1C_2}$ and $\epsilon^{A_1C_2}$ were then readjusted to give a new X^{A_1} and iterated until the calculated and experimental monomer fractions converged.

Monomer Mole Fraction and Aggregate Size for Dodecanol and *t*-Butanol in Ethane and Carbon Dioxide. Figure 7 shows the monomer mole fraction data and the SAFT correlation results plotted versus the (apparent) alcohol mole fraction for dodecanol and *tert*-butyl alcohol in ethane and carbon dioxide at 40 °C and 200 bar. The data and correlation show two distinct trends. First, the monomer mole fraction for both dodecanol and *tert*-butyl alcohol is higher in carbon dioxide than in ethane; the self-association of the alcohol is decreased in carbon dioxide because the dipole−quadrupole interaction (1:1 alcohol−CO_2 complex) inhibits the alcohol aggregation. Second, the *tert*-butyl alcohol monomer mole fraction is higher than that of dodecanol in both ethane (by a factor of about 4) and carbon dioxide (by a factor of about 2), which can be explained by steric hindrance. The methyl groups of *tert*-butyl alcohol shield the hydroxy group and hence reduce the probability (bond volume) of self-association.

As illustrated in Figure 7, agreement between SAFT and the spectroscopic data is good. The goodness of fit, however, depends on the mixture densities calculated by SAFT (ρ_n in eq 3). Data for ρ_n for dodecanol and *tert*-butyl alcohol in ethane and carbon dioxide were estimated with SAFT using the binary interaction parameter (k_{ij}) derived from phase equilibrium data. The k_{ij} for ethane + dodecanol was estimated for the ethane + dodecane system,[46−48] and the k_{ij} for carbon dioxide + dodecanol was estimated from the phase equilibria of carbon dioxide + decane.[49] Table 4 lists the association parameters derived from spectroscopic data.

Consistent with Fulton et al.,[42] the aggregate size (n_a) is estimated by assuming that association follows a simple mass-action-type expression. This stoichiometric expression relates the monomer mole-fraction (X_m) to the aggregate mole fraction (X_a).

$$nX_m \overset{K_a}{\longleftrightarrow} X_a: \quad K_a = \frac{X_a}{{X_m}^n} \quad (11)$$

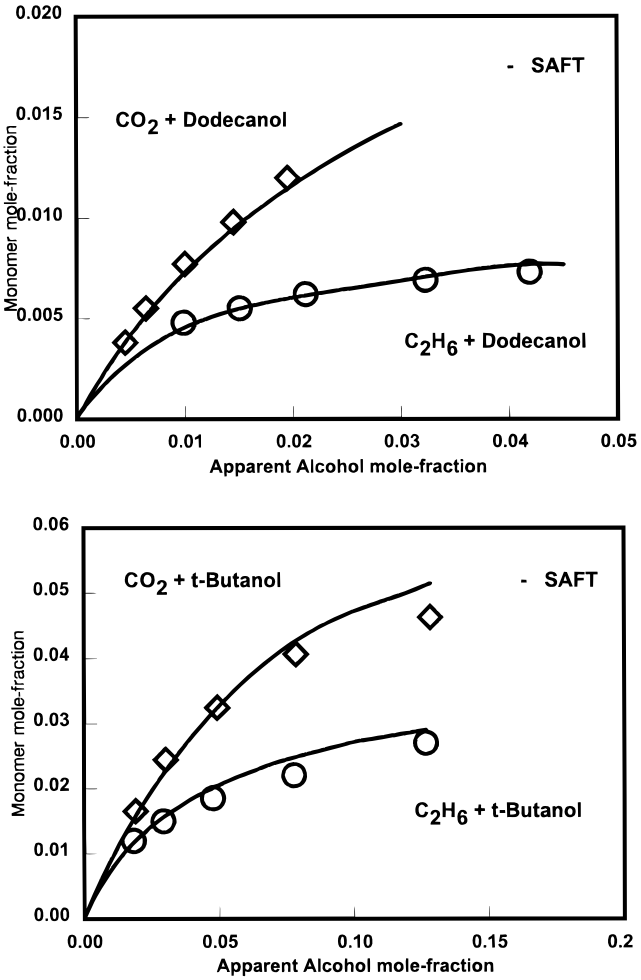

Figure 7. Monomer (free alcohol) mole fraction data for dodecanol and *tert*-butyl alcohol (2-methyl-2-propanol) in ethane (C_2H_6) and carbon dioxide (CO_2) at 40 °C and 200 bar. Experimental data are from the literature,[42] and curve was calculated using SAFT.

TABLE 5: Experimental and SAFT-Calculated Aggregate Numbers (n)

system	composition (mol fr)	press (bar)	T (°C)	n^{SAFT}	n^{EXP}
(1) C_2H_6 + dodecanol	0.020−0.080	200.0	40.0	4.4	4.5 ± 1.0^a
(2) C_2H_6 + dodecanol	0.020−0.080	200.0	120.0	2.6	
(3) C_2H_6 + *t*−butanol	0.020−0.080	200.0	40.0	3.0	3.4 ± 1.0^a
(4) C_2H_6 + dodecanol	0.006−0.030	200.0	40.0	3.0	
(5) CO_2 + dodecanol	0.006−0.030	200.0	40.0	2.4	2.8 ± 1.0^a
(6) CO_2 + *t*−butanol	0.006−0.030	200.0	40.0	2.1	

[a] Raw monomer mole fraction data from Fulton et al.[42] at 40 °C and 200 bar used to rederive the aggregate number.

From this stoichiometry and dilute solute concentrations, the equilibrium constant (K_a) can be written in terms of the total solute mole fraction ($X_t = X_m + nX_a$).

$$\ln(X_t - X_m) = n \ln(X_m) + \ln(nK_a) \qquad (12)$$

Plots of $\ln(X_t - X_m)$ versus $\ln(X_m)$ result in lines with slopes equal to n and intercepts equal to $\ln(nK_a)$. Inherent to this approach is the assumption that only an aggregate of uniform size exists; of course, the actual solution contains a distribution of dimers, trimers, and higher order aggregates.

To facilitate these plots, the SAFT model was used to calculate X_m, given X_t. Table 5 shows the agreement between the calculated (N_a^{SAFT}) and experimental (N_a^{EXP}) aggregate size for dodecanol and *tert*-butyl alcohol in ethane and carbon dioxide solutions. For example, for dodecanol in ethane solutions at 40 °C and 200 bar (line 1 in Table 5) SAFT shows that the aggregate size of dodecanol is close to that of a tetramer ($n = 4.4$), which is in agreement with the experimental value of $n = 4.5 \pm 1.0$.

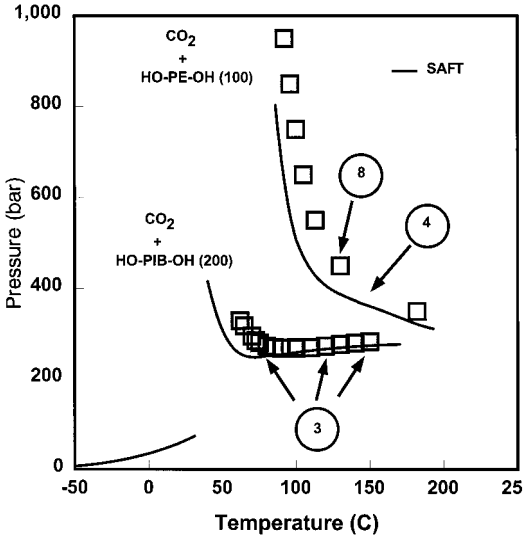

Figure 8. Binary pressure−temperature diagram for carbon dioxide (CO_2) solutions of HO−PIB−OH (200) and HO−PE-OH (100) (2,5-hexanediol). Curves and average aggregate size (in circles) calculated using SAFT with $k_{ij} = 0.132 + 2.10 \times 10^{-4}T$ (°C).

Table 5 also illustrates the effects of cross-association in carbon dioxide and of the steric hindrance of *tert*-butyl alcohol on aggregate size. For example, if ethane is replaced by carbon dioxide as the solvent (lines 4 and 5 in Table 5), the average aggregate size of dodecanol decreases from being a trimer ($n = 3.0$) to being close to a dimer ($n = 2.4$) because carbon dioxide reduces the self-association of dodecanol via quadrupole−dipole interactions. As a result of steric hindrance, the average aggregate size of *tert*-butyl alcohol in ethane ($n = 3.0$) is smaller than that of dodecanol in ethane ($n = 4.4$) at similar conditions (lines 3 and 1 in Table 5).

As expected, a decrease in temperature increases the aggregate size while a decrease in solute mole fraction decreases the aggregate size. For example, the aggregate size of dodecanol in ethane increases from $n = 2.6$ at 120 °C to $n = 4.4$ at 40 °C (compare lines 1 and 2 in Table 5). When the mole fraction range decreases from 0.02−0.080 to 0.006−0.030 (compare lines 1 and 4 in Table 5), the aggregate size decreases from $n = 4.4$ to $n = 3.0$.

Phase Behavior and Aggregation Size for HO−PIB−OH (200) and HO−PE-OH (100) in Carbon Dioxide and Ethane

Carbon Dioxide Solutions. Figure 8 shows the phase-boundary data for carbon dioxide solutions of HO−PIB−OH (200) (measured in this work) and HO−PE-OH (100).[1] The striking difference between these two data sets is that the phase boundaries for HO−PIB−OH (200) are at much lower pressures than are those for HO−PE-OH (100). This magnitude of difference is primarily due to the difference in molecular structure, the fact that HO−PIB−OH (200) has methyl groups attached in the 2, 4, and 6 position while HO−PE-OH (100) has no branches. It is hypothesized that the additional methyl groups of HO−PIB−OH (200) make the molecule stiff and bulky and sterically hinder its ability to hydrogen bond.

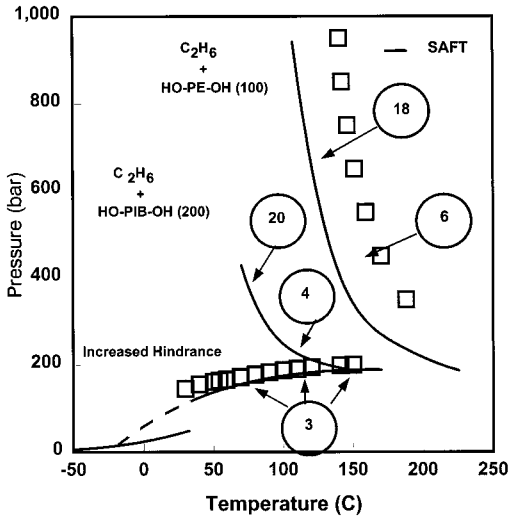

Figure 9. Binary pressure−temperature diagram for ethane (C_2H_6) solution of HO−PIB−OH (200) and HO−PE−OH (100) (2,5-hexanediol): HO−PIB−OH (200) data from this work, HO−PE−OH (100) data from the literature,[1] curve and average aggregate size (in circles) calculated using SAFT with $k_{ij} = 0.030$ (solid curve for association $\kappa = 0.0058$, dashed curve for $\kappa = 0.0029$).

To evaluate this idea, the SAFT model was used to calculate the phase boundaries for HO−PIB−OH (200) by emulating the steric hindrance using a reduced value of the associating bond volume (κ), as was done to fit the association parameters to solution spectra for *tert*-butyl alcohol. Thus, the self-association, κ, for HO−PE−OH (100) was set to 0.020, the same as that determined for dodecanol, and the self-association κ for HO−PIB−OH (200) was set to 0.0058, the same as that determined for *tert*-butyl alcohol. The self-association energy (ϵ) for both of these compounds is 2752 K (Table 4), and the binary interaction parameter used to generate both of these curves is $k_{ij} = 0.132 + 2.10e^{-4}T$ (°C).

As shown in Figure 8, the hypothesis that steric hindrance reduces κ and, hence, reduces the aggregate size results in reasonably good agreement between SAFT and the experimental data. It is also noted that, at 150 °C, the aggregate size of HO−PIB−OH (200) is 3 [≈1.5 HO−PIB−OH (200) at each hydroxy group] and the aggregate size for HO−PE−OH (100) is 4 [≈2 HO−PE−OH (100) at each hydroxy group]. Furthermore, as the temperature is lowered to 120 °C, e.g., the aggregate size of HO−PE−OH (100) increases to 8 while the aggregate size of HO−PIB−OH (200) remains essentially constant at 3.

Ethane Solutions. Figure 9 shows the binary phase boundary data for HO−PIB−OH (200) (measured in this work) and HO−PE−OH (100)[1] in ethane. Similar to the trends observed for carbon dioxide, the phase boundary for HO−PIB−OH (200) is at pressures lower that those for HO−PE−OH (100), a result of the steric hindrance effect on association, which is qualitatively captured by SAFT (solid curve). The aggregate size for HO−PE−OH (100) at 150 °C is 6 compared to the HO−PIB−OH (200) aggregate size of 3. The difference in aggregate size, and hence phase-boundary pressures, increases as the temperature is lowered to 120 °C, where the aggregate size for HO−PE−OH (100) is 18 and that for HO−PIB−OH is 4. This size difference results in a factor of about 3 in phase-boundary pressures at 150 °C.

These calculations are based on the SAFT parameters listed in Table 4 and on a k_{ij} value of 0.030 [the same value used for both HO−PE−OH (100) and HO−PIB−OH (200)].

Solvent Effect. SAFT quantitatively captures the difference in phase-boundary pressures for HO−PE−OH (100) in carbon dioxide and ethane (Figures 8 and 9). The analysis indicates that the cross-association between the carbon dioxide quadrupole (modeled as an effective SAFT site) and the hydroxy groups lowers the phase-boundary pressures relative to those for ethane solutions. This lowering is due to a decrease in HO−PE−OH (100) aggregate size in carbon dioxide. For example, at 150 °C, the aggregate size of HO−PE−OH (100) in ethane is 6 while the aggregate size for HO−PE−OH (100) in carbon dioxide is 4. This larger HO−PE−OH (100) aggregate size in ethane increases the size difference between the solute and solvent, which increases the phase-boundary pressures.

SAFT calculations indicate that carbon dioxide reduces the phase-boundary pressures also for HO−PIB−OH (200) relative to those in ethane. However, the experimental data do not support this observation. The phase-boundary pressures measured for HO−PIB−OH (200) in ethane are lower than those measured for carbon dioxide (Figure 6). To fit this behavior, κ was further reduced by 50% (from 0.0058 to 0.0029). This adjustment results in a calculated phase boundary that is type B (dashed curve labeled "Increased Hinderane" in Figure 9) with a lower critical end point (LCEP) at −17.1 °C. In the temperature range 75−150 °C, the predicted HO−PIB−OH (200) aggregate size is nearly constant at 3. On the basis of the similarities in aggregate size for HO−PIB−OH (200) in both solvents, one can conclude that the phase-boundary pressures for HO−PIB−OH (200) in carbon dioxide are higher than those in ethane because ethane is a better solvent for PIB. The fact that lower values of κ are required to fit the HO−PIB−OH (200) data in Figure 9 suggests that the hydroxy groups of HO−PIB−OH (200) are more hindered in ethane than in carbon dioxide, which leads to lower bond volumes; the methyl branches of HO−PIB−OH (200) more effectively shield the hydroxy groups in the nonpolar ethane than in the polar carbon dioxide solutions.

Conclusions

The shifts in phase boundaries for CH_3−PIB−CH_3 (200), CH_3−PIB−OH (200), and HO−PIB−OH (200) in binary solutions of ethane, carbon dioxide, and chlorodifluoromethane can be explained by intermolecular association. In ethane and carbon dioxide solutions, as the number of hydroxy groups increases, so do the phase-boundary pressures. This increase is a result of the polymer aggregation due to self-association. In chlorodifluoromethane solutions, no change in phase-boundary pressures is observed as the number of hydroxy groups increases. Cross-association between chlorodifluoromethane and the hydroxy groups prevents the polymers from aggregating.

In ethane and carbon dioxide solutions, two key differences are observed between HO−PE−OH (100) (2,5-hexanediol) and HO−PIB−OH (200): (1) in either solvent, the phase boundary pressures for HO−PIB−OH (200) are 2−3 times lower than those for HO−PE−OH (100); (2) in contrast to HO−PIB−OH (100), the cross-association between the carbon dioxide quadrupole and the HO−PE−OH (100) hydroxy groups lowers the phase-boundary pressures relative to those for ethane. The SAFT calculated phase-boundary pressures and aggregate size for HO−PE−OH (100) and HO−PIB−OH (200) indicate that (1) the methyl branches of HO−PIB−OH (200) hinder polymer aggregation and lower the phase boundary relative to that for HO−PE−OH (100) and (2) the methyl groups of HO−PIB−OH (200) more effectively shield the hydroxy groups in the nonpolar ethane than in the polar carbon dioxide, which tends to lower the phase-boundary pressures relative to those in carbon dioxide.

Acknowledgment. The authors thank Prof. Yee Chiew of Rutgers University for providing stimulating discussions on the use of SAFT for probing various associating schemes and Dr. John Fulton of Battell Pacific Northwest Laboratories for making available the experimentally measured monomer mole fraction data for supercritical fluid solutions of alcohols.

References and Notes

(1) Alwani, Z.; Schneider, G. M. *Ber. Bunsen-Ges. Phys. Chem.* **1976**, *80* (12), 1310.
(2) Zeck, S.; Knapp, H. *Fluid Phase Equilib.* **1986**, *25*, 303.
(3) Gupta, M. K.; Gardner, G. C.; Hegarty, M. J.; Kidnay, A. J. *J. Chem. Eng. Data* **1980**, *25*, 313.
(4) Li, Y.; Dillard, K. H.; Robinson, R. L., Jr. *J. Chem. Eng. Data* **1981**, *26*, 53.
(5) Wagner, Z.; Wichterle, I. *Fluid Phase Equilib.* **1987**, *33*, 109.
(6) Brennecke, J. F.; Eckert, C. A. *Supercritical Fluid Science and Technology*; Johnston, K. P., Penninger, J. M. L., Eds.; ACS Symposium Series 406; American Chemical Society: Washington, DC, 1989; p 14.
(7) Gupta, R. B.; Combes, J. R.; Johnston, K. P. *J. Phys. Chem.* **1992**, *97*, 707.
(8) Kim, S.; Johnston, K. P. *AIChE J.* **1987**, *33*, 1603.
(9) Kim, S.; Johnston, K. P. *Ind. Eng. Chem. Res.* **1987**, *26*, 1206.
(10) Nickel, D.; Schneider, G. M. *J. Chem. Thermodyn.* **1989**, *21*, 293.
(11) O'Shea, K. E.; Kirmse, K. M.; Fox, M. A.; Johnston, K. P. *J. Phys. Chem.* **1991**, *95*, 7863.
(12) Swaid, I.; Nickel, D.; Schneider, G. M. *Fluid Phase Equilib.* **1985**, *21*, 95.
(13) Anderko, A. *Fluid Phase Equilib.* **1989**, *50*, 21.
(14) Anderko, A. *Fluid Phase Equilib.* **1991**, *65*, 89.
(15) Chapman, W. G.; Gubbins, K. E.; Jackson, G.; Radosz, M. *Ind. Eng. Chem. Res.* **1990**, *29*, 1710.
(16) Gupta, R. B.; Panayiotou, C. G.; Sanchez, I. C.; Johnston, K. P. *AIChE J.* **1992**, *38*, 1243.
(17) Vimalchand, P.; Ikonomou, G. D.; Donohue, M. D. *Fluid Phase Equilib.* **1988**, *43*, 121.
(18) Braker, W.; Mossman, A. L. *Matheson Gas Data Book*, 6th ed.; Matheson Gas Products, Inc., Lyndhurst, NJ, 1980; pp 169.
(19) Kennedy, J. P.; Ross, L. R.; Lackey, J. E.; Nuyken, O. *Polym. Bull.* **1981**, *4*, 67.
(20) Faust, R.; Nagy, A.; Kennedy, J. P. *Macromol. Sci. Chem.* **1987**, *A24* (6), 595.
(21) Gregg, C. J.; Stein, F. P.; Morgan, C. K.; Radosz, M. *J. Chem. Eng. Data* **1994**, *39*, 219.
(22) Chen, S.-j.; Radosz, M. *Macromolecules* **1992**, *25*, 3089.
(23) Bresserer, G. J.; Robinson, D. B. *J. Chem. Eng. Data*. **1973**, *18* (3), 301.
(24) Lhotak, V.; Wichterle, I. *Fluid Phase Equilib.* **1981**, *6*, 229.
(25) Ohagaki, K.; Nakai, S.; Nitta, S.; Katayama, T. *Fluid Phase Equilib.* **1982**, *8*, 113.
(26) Rodrigues, A. B. J.; McCaffrey, D. S.; Kohn, J. P. *J. Chem. Eng. Data* **1968**, *13*, 164.
(27) Radosz, M. *Ind. Eng. Chem. Res.* **1987**, *26*, 2134.
(28) Enick, R.; Holder, G. D.; Morsi, B. I. *Fluid Phase Equilib.* **1985**, *22*, 209.
(29) Fall, D. J.; Luks, K. D. *J. Chem. Eng. Data* **1985**, *30*, 276.
(30) Hottovy, J. D.; Luks, K. D.; Kohn, J. P. *J. Chem. Eng. Data* **1981**, *26*, 256.
(31) Schneider, G. *Chem. Eng. Prog. Symp. Ser.* **1968**, *64*, 9.
(32) Lam, D. H.; Jangkamolkulchai, A.; Luks, K. D. *Fluid Phase Equilib.* **1990**, *60*, 131.
(33) Xu, N.; Yanru, J. Y.; Wang, Y.; Shi, J.; Lu, B., *Fluid Phase Equilib.* **1991**, *69*, 261.
(34) Gregg, C. J.; Chen, S. J.; Stein, F. P.; Radosz, M. *Fluid Phase Equilib.* **1993**, *83*, 375.
(35) Huang, S. H.; Radosz, M. *Ind. Eng. Chem. Res.* **1990**, *29*, 2284.
(36) Huang, S. H.; Radosz, M. *Ind. Eng. Chem. Res.* **1991**, *30*, 1994.
(37) Economou, I. G.; Gregg, C. J.; Radosz, M. *Ind. Eng. Chem. Res.* **1992**, *31*, 2620.
(38) Gregg, C. J.; Chen, S. J.; Stein, F. P.; Radosz, M. *Ind. Eng. Chem. Res.* **1993**, *32*, 1442.
(39) Chen, S.-j.; Econoumou, I. G.; Radosz, M. *Macromolecules* **1992**, *25*, 3089.
(40) Fulton, J. L.; Yee, G. G.; Smith, R. D. *J. Supercrit. Fluids* **1990**, *3*, 169.
(41) Fulton, J. L.; Yee, G. G.; Smith, R. D. *J. Am. Chem. Soc.* **1991**, *113*, 8327.
(42) Fulton, J. L.; Yee, G. G.; Smith, R. D. *Supercritical Fluid Engineering Science Fundamentals and Applications*; ACS Symposium Series 514; American Chemical Society: Washington, D.C., Kiran, E., Brennecke, J. F., Eds.; 1993; Vol. 514, p 175.
(43) Yee, G. G.; Fulton, J. L.; Smith, R. D. *Langmuir* **1991**, *8*, 377.
(44) Yee, G. G.; Fulton, J. L.; Smith, R. D. *J. Phys. Chem.* **1992**, *96*, 6172.
(45) Jackson, G.; Chapman, W. G.; Gubbins, K. E. *Mol. Phys.* **1988**, *62*, 843.
(46) Legret, D.; Richon, D.; Renon, H. *Ind. Eng. Chem. Fundam.* **1980**, *19*, 122.
(47) Meskel-Lesavre, M.; Richon, D.; Renon, H. *Ind. Eng. Chem. Fundam.* **1981**, *20*, 284.
(48) Reamer, H. H.; Sage, B. H. *J. Chem. Eng. Data*, **1963**, *8*, 508.
(49) Nagarajan, N.; Robinson, R. L. *J. Chem. Eng. Data* **1986**, *31*, 168.